Nano Energy (2014) 10, 305–312

Available online at www.sciencedirect.com

ScienceDirect

journal homepage: www.elsevier.com/locate/nanoenergy

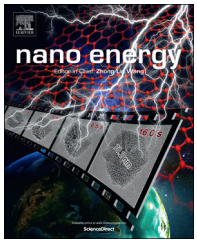

RAPID COMMUNICATION

Self-powered triboelectric velocity sensor for dual-mode sensing of rectified linear and rotary motions

Qingshen Jing[a,b], Guang Zhu[b,c], Wenzhuo Wu[b], Peng Bai[b], Yannan Xie[b], Ray P.S. Han[a,*], Zhong Lin Wang[b,c,**]

[a]Department of Materials Science and Engineering, Peking University, Beijing 100871, China
[b]School of Materials Science and Engineering, Georgia Institute of Technology, Atlanta, GA 30332-0245, United States
[c]Beijing Institute of Nanoenergy and Nanosystems, Chinese Academy of Sciences, Beijing, China

Received 10 August 2014; received in revised form 16 September 2014; accepted 17 September 2014
Available online 7 October 2014

KEYWORDS
Self-powered;
Triboelectric generator;
Velocity sensor;
Rectilinear motion;
Rotary motion

Abstract
A practical self-powered velocity sensor based on the principles of a triboelectric generator for either rectified linear or rotary motion is presented. The effort represents the first successful attempt in integrating a triboelectric generator into a commercial digital circuit for the dual-mode speed sensing. Employing alternating Kapton-copper strips arranged in a spiral configuration wrapped on the inner and outer surfaces of two concentric cylinders, voltage assays for linear and rotary motions can be measured without the need for an external power source. The triboelectric generated output signals when integrated with a digital circuit and a microcontroller unit can be directly processed into remarkably stable, macro-scale output signals for measurements of $(0.1-0.6)\ ms^{-1} \pm 0.5\%$ for linear velocities and $(300-700)\ rpm \pm 0.9\%$ for rotary velocities. We have also discussed the measuring sensitivities and limitations of our device in the paper. We believe our pioneering demonstration of the applied triboelectric technology will have a huge impact in the industrial commercialization of self-powered devices and sensors.

*Corresponding author.
**Corresponding author at: School of Materials Science and Engineering, Georgia Institute of Technology, Atlanta, GA 30332-0245, United States.
E-mail addresses: ray-han@pku.edu.cn (R.P.S. Han), zlwang@gatech.edu (Z.L. Wang).

http://dx.doi.org/10.1016/j.nanoen.2014.09.018
2211-2855/

Introduction

Velocity measurements are essential in many modern industrial applications in automation, transportation, robotics,

etc. The well-developed methods for velocity measurements include technologies based on potentiometers [1], magneto resistive sensing [2], magnetic field sensors [3], optical encoders [4], capacitive sensing [1], piezoelectric sensors [5-7], etc. Most of these sensing technologies suffer from a shortcoming: they require a power supply to sense the mechanical motion. Such sensors can be classified as passive because they cannot actively detect a change in the environment without being driven by electricity. Even for some active sensors that are designed to initially generate electrical signals [5-8], the outputs are rather small and they need a sophisticated equipment for measurement, which may prohibit their applications to some extent. The invention of the first triboelectric generator (TEG) [9] that uses the tribo-electrification and electrostatic induction effects to generate electrical output allows the technology to be applied in the harvesting of the mechanical energy [10-12] and in self-powered sensor fields such as magnetic field sensor [13], position sensors [14], acoustic sensors [15] and chemical sensors [16,17]. Theoretical studies [18] showed strong regular pattern and stability in the TEG outputs for a cost-effective mechanical sensing. Based on the theory, various types of motion sensors have been developed [19-22]. Recently, a one-dimensional nano-scale motion sensor was developed to detect nanometer-scale movements [23]. The work represents the first triboelectric-related research on velocity/position sensing in a one-dimensional array; however, the detected output voltage/current signals were micro-scale in magnitude, and thus, too small for practical applications.

We report on a practical self-powered sensor for velocity measurements for either linear or rotary motion. The effort represents the first successful attempt in integrating a triboelectric generator with a comparator-microcontroller unit (MCU) into a commercial digital circuit for the dual mode velocity sensing. Patterned with alternating Kapton-copper strips arranged in a 45°-helix on both sides of the contact surface and packed in a case-encapsulated structure, the generator produced remarkably stable, macro-scale output signals for measurements of $(0.1-0.6)$ $ms^{-1} \pm 0.5\%$ for linear velocities and $(300-700)$ rpm $\pm 0.9\%$ for rotary velocities. Our velocity sensor demonstrates the technical feasibility and commercial potential of triboelectricity for self-powered devices and sensors.

Results and discussions

The schematic and actual structures of the velocity sensing triboelectric generator (vsTEG) are shown respectively, in Figure 1a1 and a2 as consisting of a pair of coaxially-placed cylindrical tubes. The two tubes move relative to each other either in a rotational (Figure 1a3) or sliding (Figure 1a4) motion. The mechanism of the velocity sensing capability can be explained as coming from the induced triboelectric charge transfer between the interfaces and its subsequent lateral polarization as driven by the relative motion. To fabricate the interfaces, a polyimide film (Kapton®) was used not only as a durable supporting substrate but even more importantly, as a high-performance electrification material [24] for generating the triboelectric charges during the sliding motion with the copper electrodes. On either side of the Kapton film, copper stripes are deposited with a linear pitch of 8 mm. Hence, the electrode stripes on the 2 sides form a linear shift of half a pitch giving rise to an alternating pattern with one another (Figure 1b). The Kapton film is then carefully wrapped over the acrylic cylinder with the strip direction at a 45° screw-angle with the cylinder axis (Figure 1a1 and a2). A second Kapton film with the same electrode pattern is encased in the foam sleeve for producing the relative motion (Figure 1a1). It should also be mentioned that the width of each copper strip (≈ 4 mm) is significantly larger than its thickness (≈ 1 μm). As a result, the inner and outer surfaces will not encounter the problem of "non-contacting 2 plates" during the device operation. An inner electrode (IE) is formed by stringing together the copper stripes at the 2 contact surfaces via bus electrodes; likewise, an outer electrode (OE) is formed by those on the other side of the Kapton film (Figure 1c). The output signal is read from the voltage over load R in the connected IE and OE (Figure 1c).

The vsTEG begins to actively generate output signals for velocity sensing when relative linear or rotary motion between the 2 interfaces occurs. The electricity generation mechanism of the vsTEG is illustrated in Figure 2a. The triboelectric charge transfer due to the Kapton and copper being brought into contact causes the electrons to be injected between the 2 dissimilar metals generating current flow between the IE and OE (see Figure 2a1-a5). Both the motion and electric signal complete their cycles at the state in Figure 2a5 and return back to the starting cycle state in Figure 2a1. Since the generated electric signal cycle stays consistently in sync with the driving mechanical (or motion) cycle, the retrieved velocity information is both stable and reliable.

The electric signals generated by the triboelectric charge transfer due to the dynamic mismatch between the strips exist as long as there is a component of the relative velocity that is perpendiculars to the strip directions. To further understand this mechanism, open-circuit voltages (V_{oc}) as well as charge accumulations (Q_{ac}) under the short-circuit condition between the IE and the OE are studied via finite element (FE) simulations (see details in *Experiments*) in a 2-dimentional space. The V_{oc} and Q_{ac} are assumed to be functions of spatial positions and are calculated by placing a smaller layer of the treated Kapton film over a larger layer at different positions (Figure 2b) with the strip direction forming a 45° angle to both the x- and y-axes. Both V_{oc} and Q_{ac} showed a "wavy" shape distribution that is consistent with the structural variation of the strips (Figure 2c and d). FE simulations confirmed that a relative motion with a velocity component that is perpendiculars to the 45° direction generates a periodic output. Denoting θ as the angle between the direction of motion and the x-axis (Figure 2e), the cycle time of V_{oc}, T can be obtained from:

$$T = \frac{w_{pitch}}{v_{sliding}\cos(45^\circ - \theta)} \quad (1)$$

where w_{pitch} refers to the pitch distance and $v_{sliding}$ to the sliding velocity along the given θ direction. Output signal variations that correspond to θ ($0 \le \theta \le 90^\circ$) for our dual-use vsTEG design with the inner cylinder moving either linearly with $\theta = 90^\circ$ or in a rotary motion with $\theta = 0^\circ$ are studied in supporting information (SI) S1. To characterize the

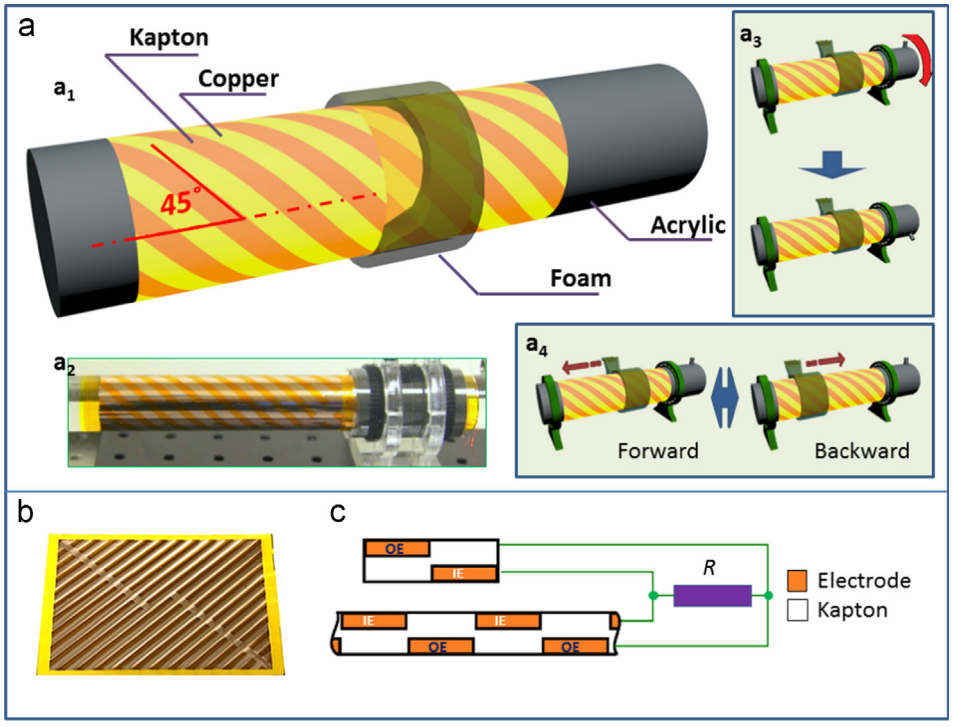

Figure 1 Rotary and linear operations of the vsTEG. (a) Schematic (a1) and actual, (a2) structure of the vsTEG for rotary, (a3) or linear reciprocating, and (a4) motion. (b) Electrodes deposited on one surface of the Kapton film are linked. (c) Electrodes between contacting surfaces are linked as inner electrodes (IE), while the rest as outer electrodes (OE).

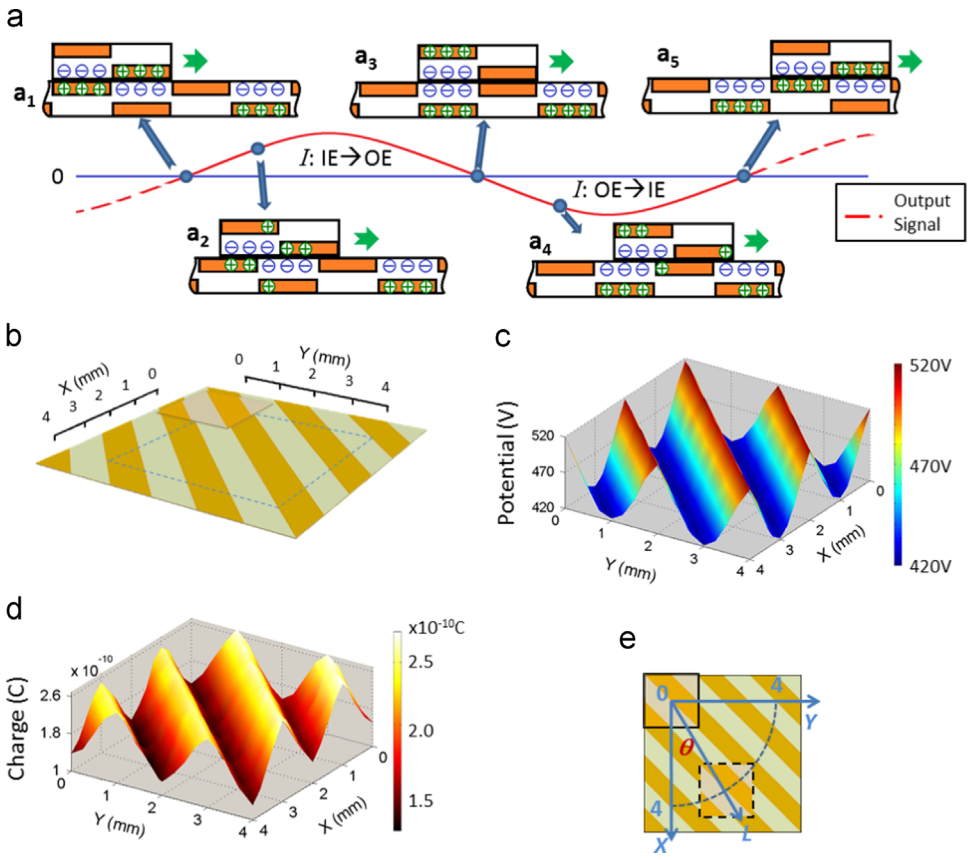

Figure 2 Working mechanism of the vsTEG and simulation of its potential/charge distribution. (a) Relationship between the output signal and the relative position change from (a1) to (a5). (b) Model simplified as a piece of film sliding over a larger piece of film within an active 4 mm × 4 mm area. (c) Simulated potential difference (V_{oc}) between IE and OE for varying positions of the smaller film. (d) Simulated charge transfer between IE and OE. (e) Motion direction as defined by θ.

performance of the vsTEG, the relationships among velocity, output voltage and external circuit load are studied (Figure 3a). A rotary vsTEG is installed by having the two ends of the inner cylinder firmly collared with bearings and rotationally driven by a motor with a 1:2 reduction ratio (Figure 3b). The outer cylinder is firmly clamped to ensure there is relative motion between the 2 coaxial cylinders. The external circuit load is adjusted by suitably tuning the load resistance. Voltage signals (V_r) are measured for varying velocities from 100–500 rpm and representative curves are plotted and categorized in Figure 3a. As shown, for a given rotational velocity, the V_r peak value increases with increasing load resistance. Similarly, for a given load resistance, the V_r peak value and intensity increase with increasing rotational velocity. For a better clarity, a 3-dimensional V_r peak value plot is sketched in Figure 3c with the velocity and load forming the 2 horizontal axes. At lower velocities and smaller loads, the V_r peaks are relatively small and difficult to distinguish from the background noise. As the load (or velocity) increases, the surface of V_r peaks approaches a relatively flat area, which is equivalent to an open circuit condition. To further examine the shape of the output signal, different V_r graphs obtained at the 3 MΩ load are plotted together for different rotational velocities in Figure 3d. As shown, V_r peak values vary from 17–31 V and they become more intense with increasing rotational velocities.

To take advantage of the cycle information, signal conversion technology is a prerequisite. A comparator (LM393N, Texas Instruments®) is applied to convert the output analog signal into the transistor-transistor logic (TTL) signal (Figure 4a). The LM393N has 2 sets of comparator integrated in a chip with each comparator containing 2 input pins (inverting and non-inverting input) and one output pin. The comparator provides the function of shifting its output level from logic high to logic low once the voltage level in inverting input exceeds the one in non-inverting input (details about LM393N are provided in S2 from SI). By choosing a proper reference voltage level applied on the non-inverting input pin, the vsTEG output signal is able to be instantaneously converted to TTL square wave with consistent timeline characters (Figure 4a). However, several concerns on the reference voltage must be considered and they include the reference level should be lower than the V_r peaks, the reference level should overcome the noise when the vsTEG is in the static state, and the converted TTL signal should be consistent with the original signal even if fluctuations at varying cycles are present. A reference level of +1 V is chosen to meet all of the considerations for later tests. By reading out each falling edge from the TTL signal

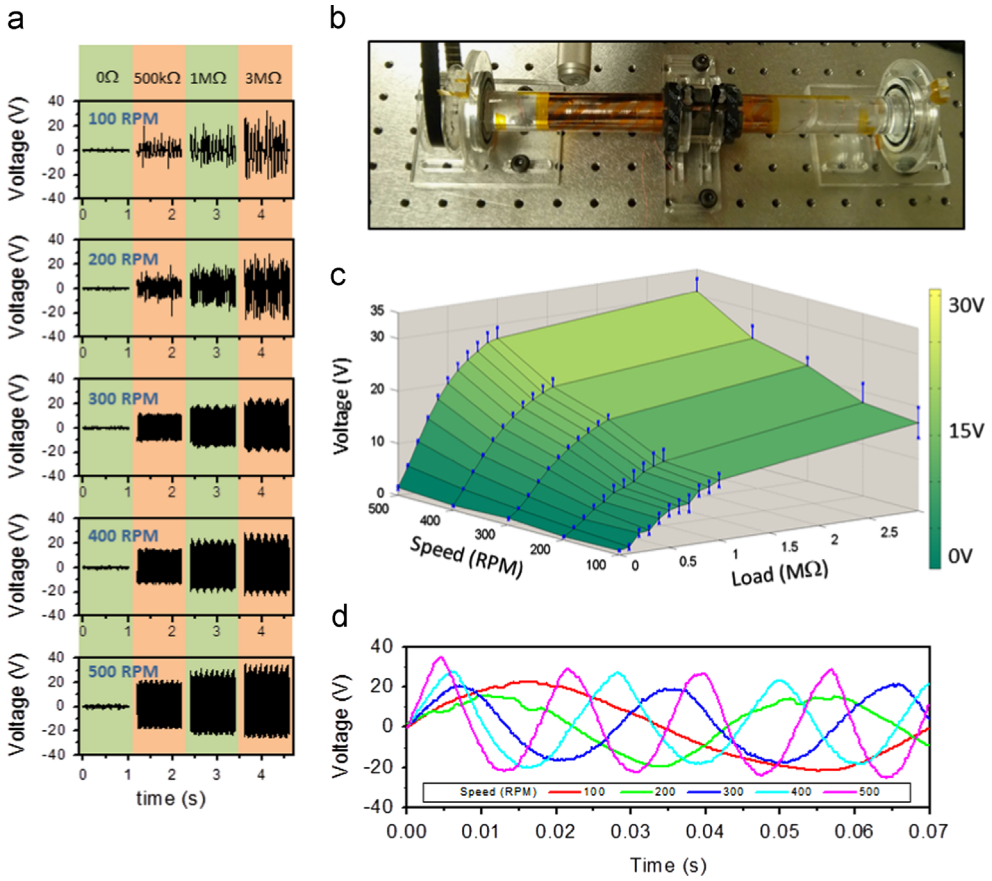

Figure 3 Output characteristics for changing velocities and external loads. (a) The vsTEG output voltage as a function of varying rotational velocity from 100 to 500 rpm and varying external load from 0 to 3 MΩ. (b) The vsTEG configured for rotary motion mode. (c) 3D plot of the relationship among the maximum output (with error bar), velocity and load. (d) Varying velocities generate varying signal cycle length (measured at the 3 MΩ load).

while maintaining the timing, the cycles are acquired and the velocities are calculated using Eq. (1) by the MCU. The circuit and flow diagrams of the system and process are given in S3 and S4 from SI.

A series of velocities are tested for the rotary motion connections (Figure 4b) with the velocity varying from 125 to 700 rpm (corresponding to the driving motor velocity of 250 to 1400 rpm). The performance of the rotary vsTEG is recorded both in image sequences (Figure 4b, Video S1) and in electrical data form (Figure 4c, S5 from SI). The data obtained and given in Figure 4c displayed a remarkable stability and accuracy with little divergence at each test point. Table S5 from SI summarizes the key results that include the "measured reduction ratio" calculated from the LED-read data, and errors for each of the tested point (see calculations in S7 from SI). As the velocity increases, the reduction ratio exhibits a slightly increasing deviation from the 1:2 mechanical reduction ratio. This difference may be attributed to the fabrication errors (see S8 from SI) and can be corrected by optimizing the computational software.

Next, the linear vsTEG is characterized using a programmable reciprocating motor with a linear motion. The outer cylinder is clamped in space and one end of the inner cylinder firmly attached to the linear motor to produce a relative linear-reciprocating motion between the 2 coaxial cylinders. The performance of the linear vsTEG for varying velocities is recorded (Video S2) and shown in Figure 5a. In contrast with the continuous output signals generated by the rotary vsTEG, the linear vsTEG showed bands output signals corresponding to the forward and backward linear motions, as well as, intermittent stop motions (Figure 5b). To minimize inaccuracies, motion that exhibits acceleration and deceleration are discarded; only the middle part of the converted TTL signals with a uniform cycle that best represents the pre-set velocity of the motor is used. The MCU is therefore, programmed accordingly and optimized for best results. The forward and backward velocities are studied separately (Figure 5c and d, Table S6 from SI) with assistance from a video camera. As shown, the velocities obtained exhibit remarkable stability and accuracy for both forward and backward motions. As the test velocity increases, the linear vsTEG begins to display a slightly increased deviation from the motor velocity (Figure 5c and 5d), which may be caused by the lag in the program. Also, the backward motion seems to possess a larger error than the forward motion (Table S6), which may be attributed to asymmetric driving condition of being pulled-pushed at only one end of the inner cylinder. However, for all the tested points, the linear vsTEG exhibited a standard error of no more than 0.5%.

Generally speaking, there are 3 factors that determine the vsTEG measuring range: the output signal amplitude, sliding spatial cycle (affected by θ) and program-allowed minimum timing interval. As the velocity decreases, the signal amplitude reduces (Figure 3c) and as it approaches the reference voltage, the comparator will exhibit a propensity for instability that will result in a distorted conversion. Thus, this factor only restricts the minimum velocity that the vsTEG can measure. Observe that the spatial cycle factor $w_{pitch}/\cos(45^\circ - \theta)$ in Eq. 1 impacts the sliding velocity in a cyclic min-max. Suppose the spatial cycle increases (by either w_{pitch} or θ), the range will be shifted to a higher value at both min-max. The processing time at the minimal sampling point determines the maximum detectable velocity. Taking into

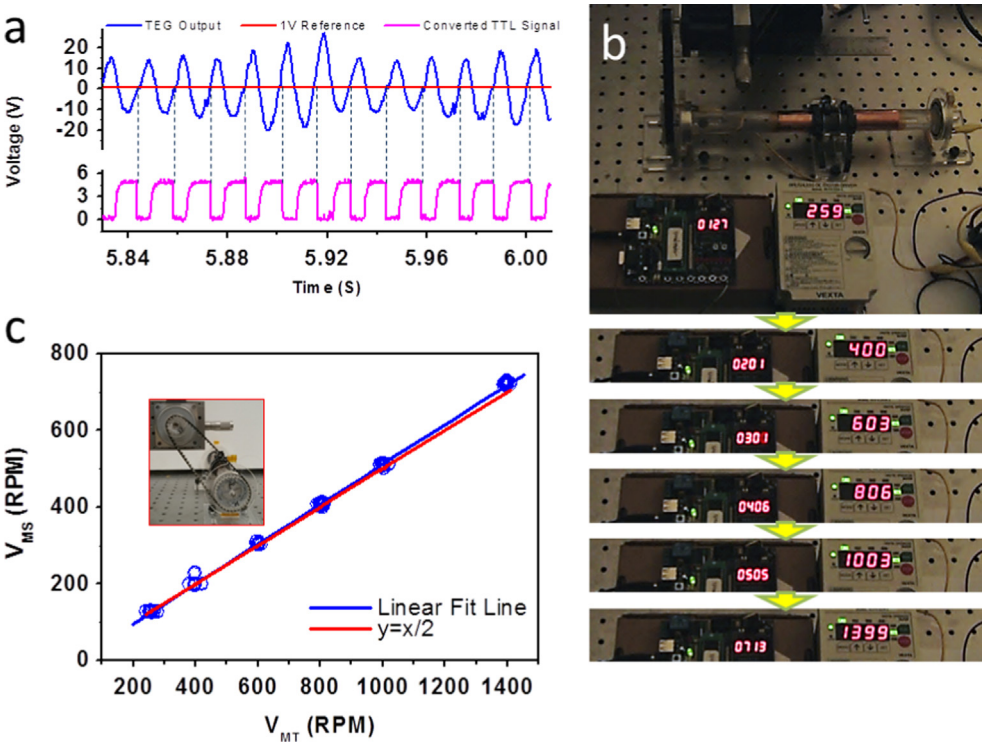

Figure 4 The rotary vsTEG. (a) Actual sample of the vsTEG signals converted into TTL signals. (b) The vsTEG setup for a reduction ratio of 1:2 rotary motion. The right-side LED displays the motor speed and the left-side depicts the vsTEG speed. (c) Data collected for varying velocities showed stable and consistent correlations.

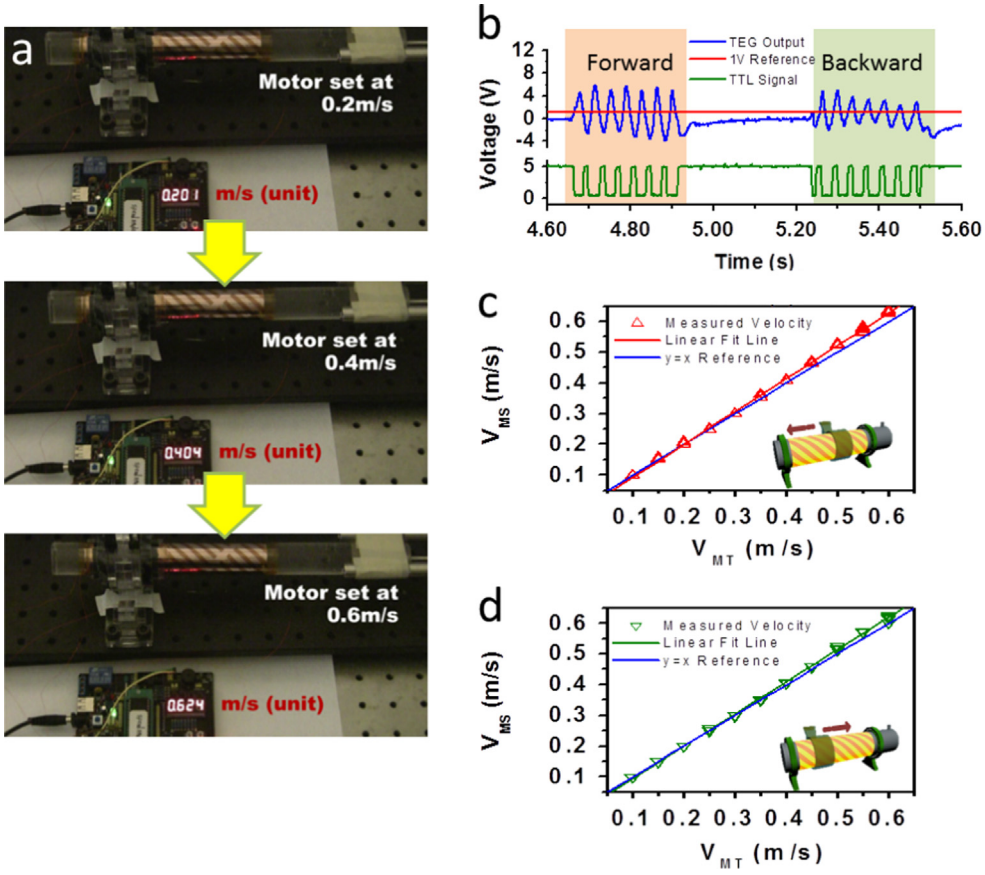

Figure 5 The linear vsTEG. (a) The vsTEG connected to a linear reciprocating motor and driven at varying linear speed from 0.1-0.6 ms^{-1}. (b) Output signals are differentiated as forward and backward with the help of a camera. (c) Forward and (d) backward motion data collected at varying velocities showed good consistency.

account the necessary considerations that include the interrupt response, interference judgment, etc., the minimal processing time in our system is about 5 ms to yield a maximum velocity of 1730 rpm and 2.3 ms^{-1} in the rotary and linear motion, respectively. Further, the response sensitivity can be determined by computing the gradient $dT/dv_{sliding}$ from Eq. 1

$$\frac{dT}{dv_{sliding}} = -\frac{w_{pitch}}{\cos(45^\circ - \theta)} \frac{1}{v_{sliding}^2} \quad (2)$$

Observe that the sensitivity is highly impacted by the magnitude of the sliding velocity; a small change in the velocity can generate an order of magnitude change in the sensitivity.

Conclusions

In summary, invoking the two principles of triboelectrification and electrostatic induction, we demonstrated the working performance of a self-powered, dual-function velocity sensor that can detect rotary and linear velocities with high stability and accuracy. The sensor is fabricated using two axially-aligned cylindrical structures coated with alternating Kapton and copper strips helical at a 45° angle with the cylinder axis. Our device is capable of measuring linear velocities of 0.1 to 0.6 ms^{-1} with an error $<0.5\%$ and rotation velocities of 300-700 rpm with an error $<0.9\%$. The typical output voltages for a 3 MΩ external load of the vsTEG vary from several volts to 30 V, which is distinguishable in the signal conversion method for a logic circuit connection. A comparator, MCU and LED digital display are applied in the circuit for signal processing and result displaying. The work reveals the possibility of utilizing a TEG as an active signal source directly connected to a logic circuit. The resulting active signal analysis enables us to develop velocity sensors, acceleration sensors, etc. for many industrial applications.

Materials and methods

Fabrication of the vsTEG

Two rectangular pieces of Kapton film (25 μm thick) were prepared with size 12 × 15 cm^2 and 12 × 5 cm^2, and surface cleaned with isopropyl alcohol. Two firm Acrylic boards (1.5 mm thick) with corresponding sizes were laser-cut with hollow stripes. These pierced boards were used as masks for electrode deposition. Hollow stripes had individual width of 4 mm and arranged 45° to the edge in a linear pitch of 8 mm, spread over the available area of two boards but keeping the un-hollow areas connected. Column across all of the stripes was also engraved to ensure deposition of a bus electrode that connected all stripe electrodes on one surface. Kapton films were covered with corresponding-sized acrylic mask on one side and were conducted with

copper electrode deposition by physical vapor deposition (PVD). Then same masks were used for the other surface of pre-treated Kapton film with a linear shift of 4 mm before conducted with the second copper deposition. Coated with thin layer of polydimethylsiloxane (PDMS) on the surface, acrylic cylinder rod with length 30 cm and diameter 2.54 cm was then wrapped with pre-treated Kapton film (larger one) as inner part. The other pre-treat Kapton film (smaller one) was then wrapped over and followed by another layer of 0.3 cm thickness foam tape. Polyethylene terephthalate (PET) film with 75 μm thickness was finally applied onto the outer surface of foam tape as a support material. In the manner of either reciprocating form or rotating form, the outer part was able to move smoothly along the inner part. Two metal bearing were mount at each end of the rod to promise necessary rotating motion, and perform as a channel conducting signal out generated from the electrodes that moves with the rod. Electrodes located between contacting surfaces were set as inner electrode (IE), while the rest that were on the back sides of Kapton films were set as outer electrode (OE). The rod and the foam tape were then separately fixed to different supporters so that they generate relative motions. To let the rod rotate, a transition kit using timing belt and timing belt pulleys was installed between the rod and a rotary motor with foam tape part static. To generate linear motions, rob was attached to linear motor while the foam tape part was kept static.

3-Dimensional potential/charge distribution simulation

"Comsol Multiphysics® 4.2" & "Matlab® 2009" were used to simulate and present the finite element analysis results. Charge density of 20 $\mu C/m^2$ was pre-applied on to the surface of Kapton domains standing for the triboelectrification charges. Relative permittivity of Kapton was set as 3.4. Potential/charge values were first simulated using "Comsol" at 289 (17×17) different spots and then extended to a 3-dimentional surface using interpolation method provided in "Matlab".

MCU related experimental and design

Texas Instrument® comparator LM393N was used as signal treatment chip while MCU development board with core computing chip STC®89C52RC was chosen as the data processing system. Reference level to the comparator was set as 1 V and adjustable by potentiometer. Other than that, all chips were communicating with TTL signal. An additional 5 V power supply was provided to operate the system. The programing language adopted was C.

Acknowledgment

Research was supported by the "Thousands Talents" Program for pioneer researcher and his innovation team, China, Beijing City Committee of science and technology Project (Z131100006013004) and the Chinese Scholarship Council via a scholarship for Q. Jing to attend the Georgia Tech – Peking University Joint Ph.D. Program at Georgia Tech.

Appendix A. Supporting material

Supplementary data associated with this article can be found in the online version at http://dx.doi.org/10.1016/j.nanoen.2014.09.018.

Reference

[1] G. Brasseur, Proc. IEEE Conf. Instrum. Meas. Technol. (1996) 1081–1086.
[2] U. Dibbern, Sens. Actuators 4 (1983) 221–227.
[3] E. Zabler, F. Heintz, R. Dietz, G. Gerlach, Sens. Actuators A Phys. 31 (1992) 54–59.
[4] A.H. Kadhim, T.K.M. Babu, D. Okelly, IEEE Trans. Instrum. Meas. 41 (1992) 486–489.
[5] Y. Hu, C. Xu, Y. Zhang, L. Lin, R.L. Snyder, Z.L. Wang, Adv. Mater. 23 (2011) 4068–4071.
[6] L. Lin, Y. Hu, C. Xu, Y. Zhang, R. Zhang, X. Wen, Z.L. Wang, Nano Energy 2 (2013) 75–81.
[7] L. Persano, C. Dagdeviren, Y. Su, Y. Zhang, S. Girardo, D. Pisignano, Y. Huang, J.A. Rogers, Nat. Commun. 4 (2013) 1633.
[8] Z.L. Wang, Adv. Mater. 24 (2012) 280–285.
[9] F.R. Fan, Z.Q. Tian, Z.L. Wang, Nano Energy 1 (2012) 328–334.
[10] Z.L. Wang, ACS Nano 7 (2013) 9533–9557.
[11] S. Wang, L. Lin, Z.L. Wang, Nano Lett. 12 (2012) 6339–6346.
[12] G. Zhu, J. Chen, Y. Liu, P. Bai, Y.S. Zhou, Q. Jing, C. Pan, Z.L. Wang, Nano Lett. 13 (2013) 2282–2289.
[13] Y. Yang, L. Lin, Y. Zhang, Q. Jing, T.-C. Hou, Z.L. Wang, ACS Nano 6 (2012) 10378–10383.
[14] Y. Hu, J. Yang, Q. Jing, S. Niu, W. Wu, Z.L. Wang, ACS Nano 7 (2013) 10424–10432.
[15] J. Yang, J. Chen, Y. Liu, W. Yang, Y. Su, Z.L. Wang, ACS Nano 8 (2014) 2649–2657.
[16] Z.-H. Lin, G. Zhu, Y.S. Zhou, Y. Yang, P. Bai, J. Chen, Z.L. Wang, Angew. Chem. Int. Ed. 52 (2013) 5065–5069.
[17] H. Zhang, Y. Yang, Y. Su, J. Chen, C. Hu, Z. Wu, Y. Liu, C.P. Wong, Y. Bando, Z.L. Wang, Nano Energy 2 (2013) 693–701.
[18] S. Niu, Y. Liu, S. Wang, L. Lin, Y.S. Zhou, Y. Hu, Z.L. Wang, Adv. Mater. 25 (2013) 6184–6193.
[19] M. Chen, X. Li, L. Lin, W. Du, X. Han, J. Zhu, C. Pan, Z.L. Wang, Adv. Funct. Mater. 24 (2014) 5059–5066.
[20] L. Lin, S. Wang, S. Niu, C. Liu, Y. Xie, Z.L. Wang, ACS Appl. Mater. Interfaces 6 (2014) 3031–3038.
[21] W. Yang, J. Chen, X. Wen, Q. Jing, J. Yang, Y. Su, G. Zhu, W. Wu, Z.L. Wang, ACS Appl. Mater. Interfaces 6 (2014) 7479–7484.
[22] Y. Su, G. Zhu, W. Yang, J. Yang, J. Chen, Q. Jing, Z. Wu, Y. Jiang, Z.L. Wang, ACS Nano 8 (2014) 3843–3850.
[23] Y.S. Zhou, G. Zhu, S. Niu, Y. Liu, P. Bai, Q. Jing, Z.L. Wang, Adv. Mater. 26 (2013) 1719–1724.
[24] Q. Jing, G. Zhu, P. Bai, Y. Xie, J. Chen, R.P.S. Han, Z.L. Wang, ACS Nano 8 (2014) 3836–3842.

Qingshen Jing is a Ph.D. student majored in Materials Science and Technology. He is currently a Ph.D. student under the Peking University-Georgia Institute of Technology Joint Ph.D. program. His research interests focus on piezoelectric nanogenerators, triboelectric nanogenerators and active sensors.

Guang Zhu is a postdoctoral fellow in Professor Zhong Lin Wang's group at Georgia Institute of Technology. He received his B.S. degree in Materials Science and Engineering from Beijing University of Chemical Technology in 2008, and his Ph.D. degree in Materials Science and Engineering from the Georgia Institute of Technology in 2013. His research areas include synthesis and characterization of nanomaterials, mechanical energy harvesting, self-powered electronics, and micro-fabricated transducers for energy applications.

Wenzhuo Wu is the postdoctoral fellow in School of Materials Science and Engineering at Georgia Institute of Technology. He received his B.S. in Electronic Information Science and Technology in 2005 from the University of Science and Technology of China (USTC), Hefei and his M. Eng. in Electrical and Computer Engineering from the National University of Singapore (NUS) in 2008. After working at Chartered Semiconductor Manufacturing (now Global Foundries) in Singapore from 2007 to 2008, he began the doctoral research under the supervision of Prof. Zhong Lin Wang and received his Ph.D. from Georgia Institute of Technology in Materials Science and Engineering in 2013. Wenzhuo's research interests include synthesis, fabrication and integration of nanomaterials/devices; nanotechnology-enabled applications in energy harvesting/conversion/storage, electronics, optoelectronics, sensing and interfacing; piezotronics/piezo-phototronics; self-powered micro/nano-systems.

Peng Bai received his B.S. degree in Mechanical Engineering from Tsinghua University, China, in 2010. He is a Ph.D. candidate at Department of Mechanical Engineering, Tsinghua University. From 2012 to 2014, he was a visiting student in Zhong Lin Wang's group at Georgia Institute of Technology. His research interests include triboelectric nanogenerators and electronic packaging, designs and applications of triboelectric nanogenerators.

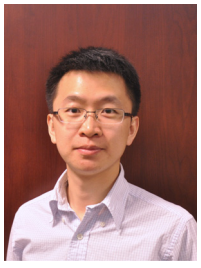

Yannan Xie is a Ph.D. candidate in Department of Physics at Xiamen University and also a visiting student in Zhong Lin Wang's group in School of Materials Science and Engineering at Georgia Institute of Technology. His research interests focus on nanomaterials synthesis, nanogenerators, self-powered systems, and optoelectronic devices.

Ray P.S. Han received his Ph.D. from the University of British Columbia, Canada. He is a Chang Jiang Chair professor in Materials Science and Engineering and as Assistant Dean of Engineering at the College of Engineering at Peking University, Beijing, China. His research interests encompass micro-nanodevices, mechanobiology, microfluidics, biomaterials, and mechanics of materials. Prior to returning back to China in 2003, he was a professor at the University of Iowa, USA for over 10 years.

Zhong Lin (ZL) Wang received his Ph.D. from Arizona State University in physics. He is the Hightower Chair in Materials Science and Engineering, Regents' Professor, Engineering Distinguished Professor and Director, Center for Nanostructure Characterization, at Georgia Tech. Dr. Wang has made original and innovative contributions to the synthesis, discovery, characterization and understanding of fundamental physical properties of oxide nanobelts and nanowires, as well as applications of nanowires in energy sciences, electronics, optoelectronics and biological science. His discovery and breakthroughs in developing nanogenerators established the principle and technological road map for harvesting mechanical energy from environment and biological systems for powering a personal electronics. His research on self-powered nanosystems has inspired the worldwide effort in academia and industry for studying energy for micro-nano-systems, which is now a distinct disciplinary in energy research and future sensor networks. He coined and pioneered the field of piezotronics and piezo-phototronics by introducing piezoelectric potential gated charge transport process in fabricating new electronic and optoelectronic devices. Details can be found at: http://www.nanoscience.gatech.edu.